LBL-27009
Preprint

Lawrence Berkeley Laboratory
UNIVERSITY OF CALIFORNIA

RECEIVED
LAWRENCE
BERKELEY LABORATORY

JAN 3 1990

LIBRARY AND
DOCUMENTS SECTION

Submitted to Journal of Magnetic Resonance

Discrete Analysis of Stochastic NMR – II

S.T.S. Wong, M.S. Roos, R.D. Newmark, and T.F. Budinger

March 1989

TWO-WEEK LOAN COPY
This is a Library Circulating Copy
which may be borrowed for two weeks.

Donner Laboratory
Biology & Medicine Division

LBL-27009 c.2

Prepared for the U.S. Department of Energy under Contract Number DE-AC03-76SF00098.

DISCLAIMER

This document was prepared as an account of work sponsored by the United States Government. While this document is believed to contain correct information, neither the United States Government nor any agency thereof, nor the Regents of the University of California, nor any of their employees, makes any warranty, express or implied, or assumes any legal responsibility for the accuracy, completeness, or usefulness of any information, apparatus, product, or process disclosed, or represents that its use would not infringe privately owned rights. Reference herein to any specific commercial product, process, or service by its trade name, trademark, manufacturer, or otherwise, does not necessarily constitute or imply its endorsement, recommendation, or favoring by the United States Government or any agency thereof, or the Regents of the University of California. The views and opinions of authors expressed herein do not necessarily state or reflect those of the United States Government or any agency thereof or the Regents of the University of California.

Discrete Analysis of Stochastic NMR – II

S.T.S. Wong, M.S. Roos, R.D. Newmark and T.F. Budinger

Donner Laboratory, Lawrence Berkeley Laboratory, University of California,

Berkeley, CA 94720

Sam T. S. Wong

Department of Radiology

Brigham and Women's Hospital

Harvard Medical School

75 Francis St.

Boston, MA 02115

Abstract

Stochastic NMR is an efficient technique for high field *in vivo* imaging and spectroscopic studies where the peak RF power required may be prohibitively high for conventional pulsed NMR techniques. A stochastic NMR experiment excites the spin system with a sequence of RF pulses where the flip angles or the phases of the pulses are samples of a discrete stochastic process. In a previous paper the stochastic experiment was analyzed and analytic expressions for the input-output cross-correlations, average signal power and signal spectral density were obtained for a general stochastic RF excitation. In this paper specific cases of excitation with random phase, fixed flip angle and excitation with two random components in quadrature are analyzed. The input-output cross-correlation for these two types of excitations are shown to be Lorentzian. Line broadening is the only spectral distortion as the RF excitation power is increased. The systematic noise power is inversely proportional to the number of data points N used in the spectral reconstruction. The use of a complete maximum length sequence (MLS) may improve the signal-to-systematic-noise ratio by 20dB relative to random binary excitation, but peculiar features in the higher order auto-correlations of MLS cause noise-like distortion in the reconstructed spectra when the excitation power is high. The amount of noise-like distortion depends on the choice of the MLS generator.

Introduction

In all previous stochastic NMR studies (*1-16*), the RF excitation vector was assumed to lie along one axis in the rotating frame with the flip angle being a Gaussian white noise or a random binary sequence. The theoretical and experimental results presented in Part I (*17*) show that fixing the phase of the RF vector causes a notch artifact, a shift in the resonance offset and a non-uniform response across the spectrum. The spectral distortions can be made negligible by reducing the RF excitation power, but the maximum signal-to-noise (S/N) ratio may not be achieved. The advent of versatile RF transmitters allows other schemes for stochastic excitation. Two excitation schemes will be discussed in this paper: random quadrature excitation and random phase excitation. The first scheme excites the spin system with RF pulses that have two statistically independent random orthogonal components. The second scheme utilizes RF pulses that have a fixed flip angle and a uniformly distributed random phase. It will be shown that both schemes produce a predictable line broadening as the only spectral distortion, as the excitation power is increased.

Closed form expressions for the first order input-output cross-correlation, average signal power and the signal power spectrum will be derived for the two excitation schemes. These expressions will be used to investigate the following aspects of the stochastic experiment: (1) The conditions under which the first order input-output cross-correlation will be a faithful estimate of the FID obtained by a conventional pulsed FT-NMR experiment, (2) the saturation behavior when the excitation power is high, (3) the experimental parameters that maximize the S/N ratio, and (4) evaluation of the signal power spectrum as an alternative estimate of the real spectrum. As in Part I, the assumptions of an isolated spin system and ergodic behavior are required. All RF pulses are assumed to be short relative to relaxation times.

Due to the stochastic nature of the experiment, all quantities estimated from the stochastic input and output of the system should be regarded as random variables. The input-output cross-

correlation, whose Fourier transform is an estimator of the spectrum, is one such quantity. The variance of the estimator, denoted as systematic noise, is usually non-white and may show up as structural artifacts. The overall noise level is determined by the sum of the systematic noise and the measurement noise from the sample and electronic hardware. It is important to keep the systematic noise level below the measurement noise level so that structural artifacts are not observed. Three sections are devoted to the analysis of systematic noise. An explanation of the nonlinear systematic noise associated with binary MLS excitation reported by Blümich and Ziessow (*8*) will also be presented.

Random Quadrature Excitation

In this section, assume that the RF vector has two orthogonal components, $\alpha_x(n)$ and $\alpha_y(n)$, that are random, statistically independent and with identical probability distributions. The excitation sequence, written as $\boldsymbol{\alpha}(n) = [\alpha_x(n), \alpha_y(n), 0]^T$, must also satisfy two conditions. The first condition is that $\alpha_x(n)$ and $\alpha_y(n)$ each have an even probability density function. This implies that they have zero mean values. For the case of non-zero mean excitation see reference (*19*). The second condition is that $\alpha_x(n)$ and $\alpha_y(n)$ are white:

$$\langle \alpha_j(n)\, \alpha_j(m) \rangle = \frac{\alpha^2}{2}\, \delta_{nm}$$

where $j = x$ or y, $\alpha^2 = \langle \boldsymbol{\alpha}(n)^T \boldsymbol{\alpha}(n) \rangle$ is the average excitation power and δ_{nm} is the Kronecker delta function.

Define the RF magnitude and phase, respectively, as

$$\beta(n) = \sqrt{\alpha_x^2(n) + \alpha_y^2(n)} \qquad [1]$$

and

$$\phi(n) = \tan^{-1}\left[\frac{\alpha_y(n)}{\alpha_x(n)}\right].$$

With the assumption of short RF duration, the RF rotation matrix $\boldsymbol{R}_\alpha(n)$ is

$$\boldsymbol{R}_\alpha(n)$$

$$= \begin{bmatrix} \cos\phi(n) & -\sin\phi(n) & 0 \\ \sin\phi(n) & \cos\phi(n) & 0 \\ 0 & 0 & 1 \end{bmatrix} \begin{bmatrix} 1 & 0 & 0 \\ 0 & \cos\beta(n) & \sin\beta(n) \\ 0 & -\sin\beta(n) & \cos\beta(n) \end{bmatrix} \begin{bmatrix} \cos\phi(n) & \sin\phi(n) & 0 \\ -\sin\phi(n) & \cos\phi(n) & 0 \\ 0 & 0 & 1 \end{bmatrix}$$

$$= \begin{bmatrix} \cos^2\phi(n) + \sin^2\phi(n)\cos\beta(n) & \cos\phi(n)\sin\phi(n)(1-\cos\beta(n)) & -\sin\phi(n)\sin\beta(n) \\ \cos\phi(n)\sin\phi(n)(1-\cos\beta(n)) & \sin^2\phi(n) + \cos^2\phi(n)\cos\beta(n) & \cos\phi(n)\sin\beta(n) \\ \sin\phi(n)\sin\beta(n) & -\cos\phi(n)\sin\beta(n) & \cos\beta(n) \end{bmatrix} \quad [2]$$

which has a mean

$$\boldsymbol{\mu}_R = \begin{bmatrix} \mu_1 & 0 & 0 \\ 0 & \mu_1 & 0 \\ 0 & 0 & \mu_2 \end{bmatrix} \quad [3]$$

where

$$\mu_1 = \langle \cos^2\phi(n) + \sin^2\phi(n)\cos\beta(n) \rangle = \langle \sin^2\phi(n) + \cos^2\phi(n)\cos\beta(n) \rangle \quad [4]$$

and

$$\mu_2 = \langle \cos\beta(n) \rangle. \quad [5]$$

From Part I Eq. [I-7] the mean magnetization is

$$\boldsymbol{\mu}_M = \frac{M_e(1-E_1)\mu_2}{1-E_1\mu_2} \begin{bmatrix} 0 \\ 0 \\ 1 \end{bmatrix}. \quad [6]$$

Combining Eqs. [I-5], [I-12] and [6] gives

$$\boldsymbol{A} = \frac{M_e(1-E_1)\mu_3}{1-E_1\mu_2} \begin{bmatrix} 0 & -1 & 0 \\ 1 & 0 & 0 \\ 0 & 0 & 0 \end{bmatrix} \quad [7]$$

where

$$\mu_3 = \langle \alpha_x(n) \cos\phi(n) \sin\beta(n) \rangle = \langle \alpha_y(n) \sin\phi(n) \sin\beta(n) \rangle. \qquad [8]$$

The estimate of the spectrum, $K_1(\omega)$, is given by Eq. [I-15]:

$$K_1(\omega) = \frac{2i\, M_e\,(1-E_1)\mu_3}{\alpha^2(1-E_1\mu_2)} \frac{1}{1-E_2\mu_1\, e^{i(\omega T_R-\theta)}}. \qquad [9]$$

Notice that $K_1(\omega)$ has only 1 pole at $\omega = \theta/T_R = 2\pi\nu$, which is the resonance offset of the spin. This implies that the line is Lorentzian centered at the expected resonance offset. The only deviation in the line shape from that obtained by a conventional FT-NMR experiment with a long interpulse delay is the line width:

$$\frac{1}{\pi T_2} - \frac{1}{\pi T_R} \log \mu_1.$$

The second term is a line broadening that varies with the excitation power. It is important to notice that the line height and line shape are independent of θ. The dephasing in the interpulse interval, θ, determines only the line location.

The covariance matrix of the magnetization vector is obtained from Eq. [I-17]:

$$\begin{aligned} \langle M\, M^T \rangle &= \frac{M_e^2(1-E_1)^2}{1-E_2^2(p_1+p_2)-E_1^2 p_4 + E_1^2 E_2^2(p_1p_4+p_2p_4-2p_3^2)} \\ &\quad \times \frac{1+E_1\cos\alpha}{1-E_1\cos\alpha} \begin{bmatrix} p_3 & 0 & 0 \\ 0 & p_3 & 0 \\ 0 & 0 & p_4 - E_2^2(p_1p_4+p_2p_4-2p_3^2) \end{bmatrix}. \end{aligned} \qquad [10]$$

where

$$\begin{aligned} p_1 &= \langle [\cos^2\phi(n) + \sin^2\phi(n)\cos\beta(n)]^2 \rangle = \langle [\sin^2\phi(n) + \cos^2\phi(n)\cos\beta(n)]^2 \rangle, \\ p_2 &= \langle \cos^2\phi(n)\sin^2\phi(n)\,[1-\cos\beta(n)]^2 \rangle, \\ p_3 &= \langle \sin^2\phi(n)\sin^2\beta(n) \rangle \qquad \text{and} \\ p_4 &= \langle \cos^2\beta(n) \rangle. \end{aligned}$$

The average signal power is the sum of the first two diagonal elements of $\langle M\, M^T \rangle$:

$$P = M_e^2\,(1-E_1)^2\,\frac{1+E_1\mu_2}{1-E_1\mu_2}\,\frac{2p_3}{1-E_2^2(p_1+p_2)-E_1^2p_4+E_1^2E_2^2(p_2p_4+p_2p_4-2p_3^2)}. \qquad [11]$$

The average signal power P is not a function of θ, which shows that the response is uniform across the spectrum.

The signal power spectrum can be obtained by combining Eqs. [I-23] and [10]:

$$\begin{aligned} S(\omega) &= 2P\,\mathcal{R}e\left\{\frac{1}{1-E_2\mu_1\,e^{i(\omega T_R-\theta)}}\right\}-P \\ &= \frac{(1-E_2^2\mu_1^2)P}{1-2E_2\mu_1\cos(\omega T_R-\theta)+E_2^2\mu_1^2} \end{aligned} \qquad [12]$$

where Re$\{\}$ means the real part of the complex quantity inside the braces. Comparing $S(\omega)$ with $K_1(\omega)$ in Eq. [9] reveals that $S(\omega)$ closely resembles the real part of $K_1(\omega)$. Therefore, the signal power spectrum is an accurate estimate of the real spectrum. The advantage of using the power spectrum is that it is calculated directly from the signal sequence.

When $\alpha_x(n)$ and $\alpha_y(n)$ are identically distributed, zero mean Gaussian white noise sequences with a variance α^2, we have

$$\begin{aligned} \mu_1 &= 1-g(\frac{\alpha^2}{4}), \\ \mu_2 &= 1-2\,g(\frac{\alpha^2}{4}), \\ \mu_3 &= \frac{\alpha^2}{4}+(1-\frac{\alpha^2}{2})\,g(\frac{\alpha^2}{4}), \\ p_1 &= 1-\frac{1}{2}\,g(\frac{\alpha^2}{4})-\frac{3}{8}\,g(2\alpha^2), \\ p_2 &= \frac{1}{2}\,g(\frac{\alpha^2}{4})-\frac{1}{8}\,g(2\alpha^2), \\ p_3 &= \frac{1}{3}\,g(2\alpha^2), \\ p_4 &= 1-g(2\alpha^2), \end{aligned}$$

where

$$g(x) = x\,e^{-x}\,{}_1F_1(\frac{1}{2},\frac{3}{2};x)$$

and ${}_1F_1$ is a degenerate hypergeometric function (*18*) defined as

$$ {}_1F_1(a,b;x) = 1 + \frac{a}{b}\frac{x}{1!} + \frac{a(a+1)}{b(b+1)}\frac{x^2}{2!} + \frac{a(a+1)(a+2)}{b(b+1)(b+2)}\frac{x^3}{3!} + \cdots \ . $$

The corresponding line shapes of $K_1(\omega)$ and $S(\omega)$ are shown in Figs. 1a and 1b respectively. Notice that line broadening is the only spectral distortion as the flip angle is increased, and $S(\omega)$ closely resembles $K_1(\omega)$ (see Figs. 4 and 8 of Part I). Figure 1c is a plot of the average signal power as a function of α. It has a peak at 1.15°. This means that the RMS flip angle that gives the maximum S/N ratio, α_{max}, is approximately the Ernst angle (see Fig.7 of Part I).

Random Phase Excitation

Random phase excitation is a special case of random quadrature excitation. It is obtained by setting the RF magnitude, $\beta(n)$, in Eq. [1], to a constant flip angle α and assuming that the RF phase, $\phi(n)$, is uniformly distributed from $-\pi$ to π. The results obtained for random quadrature excitation are applicable, but now

$$
\begin{aligned}
\mu_1 &= \cos^2\frac{\alpha}{2}, \\
\mu_2 &= \cos\alpha, \\
\mu_3 &= \frac{\alpha}{2}\sin\alpha, \\
p_1 &= \frac{1}{8}(3 + 2\cos\alpha + 3\cos^2\alpha), \\
p_2 &= \frac{1}{8}(1 - \cos\alpha)^2, \\
p_3 &= \frac{1}{2}\sin^2\alpha \qquad \text{and} \\
p_4 &= \cos^2\alpha.
\end{aligned}
$$

The plots of $K_1(\omega)$, P and $S(\omega)$ for random phase excitation are almost identical to those for random quadrature excitation with Gaussian white noise and so will not be shown here. The discussion in the previous section regarding the line shape, line distortion and optimum excitation

power also applies.

The probability distribution of the RF phase, $\phi(n)$, is not necessarily continuous. For example, $\phi(n)$ may take on the values, $\pm 45°$ and $\pm 135°$, each with a probability of 1/4. This can be implemented easily by using two independent binary maximum length sequences. The quaternary output of the MLS generators is then used to select four possible RF phases. This means that spectrometers that perform quadrature RF phase cycling may easily be modified to implement random phase excitation.

Systematic Noise and Measurement Noise

The input-output cross-correlation and the signal power spectrum have been defined in terms of the expectation operator of probability theory. In practice, ergodicity is assumed and the expectation operator is approximated by a time average. For example, the cross-correlation of two processes, $x(n)$ and $y(n)$, is estimated by

$$\langle x(n)\, y^*(n-m)\rangle \approx \frac{1}{N}\sum_{n=0}^{N-1} x(n)\, y^*(n-m). \qquad [13]$$

The approximation becomes an equality only when N approaches infinity, but in reality N is limited. Since the observed $x(n)$ and $y(n)$ are samples of two stochastic processes, the time average defined on the right hand side of the equation above will also be a sample of a stochastic process and in general will have a non-zero variance. This variance will usually appear as colored noise in the time average, and it is referred to as systematic noise. In addition to the systematic noise, the observed $x(n)$ and $y(n)$ also have measurement noise from the sample and the electronic hardware involved in the sampling process. To avoid structural artifacts resulting from the systematic noise, it is necessary to find experimental parameters such that the measurement noise is the dominant noise source. The following three sections will investigate how the measurement noise and the systematic noise decrease as N is increased. Gaussian white noise excitation and MLS excitation

will be compared with regard to systematic noise generation.

First consider the case without measurement noise. In the previous sections the Fourier transforms of the input-output cross-covariance and the signal auto-covariance were used to estimate the spectrum. From Eqs. [I-8], [I-18] and [13] the time average estimators of the input-output cross-covariance and the signal auto-covariance are, respectively,

$$k_1^N(m) = \frac{1}{N\alpha^2} B^\dagger \left\{ \sum_{n=0}^{N-1} [M(n) - \mu_M][\alpha(n-m) - \mu_\alpha]^T \right\} B \qquad [14]$$

and

$$r^N(m) = \frac{1}{N} B^\dagger \left\{ \sum_{n=0}^{N-1} [M(n) - \mu_M][M(n-m) - \mu_M]^T \right\} B, \qquad [15]$$

where the superscript N denotes the dependence on N. It is obvious that $\langle k_1^N(m) \rangle = k_1(m)$ and $\langle r^N(m) \rangle = r(m)$, i.e., they are unbiased estimators. The variances of $k_1^N(m)$ and $r^N(m)$ are defined as

$$Var\{k_1^N(m)\} = \langle |k_1^N(m)|^2 \rangle - |k_1(m)|^2 \qquad [16]$$

and

$$Var\{r^N(m)\} = \langle |r^N(m)|^2 \rangle - |r(m)|^2. \qquad [17]$$

In practice, the acquired data include measurement noise from both the sample and electronic hardware. In most cases, the measurement noise is Gaussian white noise. When representing the transverse magnetization $M_{xy}(n)$, or the signal, as a complex sequence, the measurement noise can be represented as $\mathcal{N}_x(n) + i\mathcal{N}_y(n)$ where $\mathcal{N}_x(n)$ and $\mathcal{N}_y(n)$ are independent and identically distributed Gaussian white noises with a variance of $\sigma^2/2$, so that the noise power is σ^2. In general, it is safe to assume that the measurement noise is independent of the stochastic excitation sequence $\alpha(n)$, and hence independent of the transverse magnetization. Define the noise vector as $\mathcal{N}(n) = [\mathcal{N}_x(n), \mathcal{N}_y(n), 0]$. An estimator of the input-output cross-covariance with the measurement noise

included is

$$\tilde{k}_1^N(m) = \frac{1}{N\alpha^2} B^\dagger \left\{ \sum_{n=0}^{N-1} [M(n) + \mathcal{N}(n) - \mu_M][\alpha(n-m) - \mu_\alpha]^T \right\} B. \qquad [18]$$

Since the measurement noise and the excitation sequence are independent, the estimator is unbiased, i.e. $\langle \tilde{k}_1^N(m) \rangle = k_1(m)$. From Eq. [18], the variance of the estimator is

$$\begin{aligned} Var\{\tilde{k}_1^N(m)\} &= \langle |\tilde{k}_1^N(m)|^2 \rangle - |k_1(m)|^2 \\ &= Var\{k_1^N(m)\} + \frac{\sigma^2}{N\alpha^2}. \end{aligned} \qquad [19]$$

The total noise power in the estimate of the FID consists of a systematic noise term and a measurement noise term. The systematic noise is generally not white. To avoid structural artifacts resulting from the systematic noise, it is necessary to find the right parameters and experimental setup such that the measurement noise is the dominant noise source. As in conventional FT-NMR, Eq. [19] shows that the measurement noise term is inversely proportional to the number of data points, N, used in the reconstruction. It will be shown in the next section that the systematic noise power is also inversely proportional to N, so that increasing N does not change the relative amount of the systematic and measurement noise power. It will be necessary to employ other means to make the measurement noise the dominant noise source.

An estimator for the signal auto-covariance with the measurement noise included is

$$\tilde{r}^N(m) = \frac{1}{N} B^\dagger \left\{ \sum_{n=0}^{N-1} [M(n) + \mathcal{N}(n) - \mu_M][M(n-m) + \mathcal{N}(n-m) - \mu_M]^T \right\} B. \qquad [20]$$

The mean of this estimator is given by

$$\langle \tilde{r}^N(m) \rangle = \begin{cases} r(m) + \sigma^2 & \text{if } m = 0 \\ r(m) & \text{otherwise.} \end{cases} \qquad [21]$$

The bias term is a delta function with height σ^2 at $m = 0$. The Fourier transform of $r(m)$ is the signal power spectrum, $S(\omega)$. Since the Fourier transform operator and the expectation operator are commutative the Fourier transform of both sides of the above equation gives

$$\langle \tilde{S}^N(\omega) \rangle = S(\omega) + \sigma^2 \qquad [22]$$

where $\tilde{S}^N(\omega)$ is an estimator for the signal power spectrum. Therefore, the bias term is just a DC offset in the signal power spectrum. The variance of the estimator for the signal auto-covariance is

$$\begin{aligned} Var\{\tilde{r}^N(m)\} &= \begin{cases} \langle|\tilde{r}^N(m)|^2\rangle - |r(m)+\sigma^2|^2 & \text{if } m=0 \\ \langle|\tilde{r}^N(m)|^2\rangle - |r(m)|^2 & \text{otherwise} \end{cases} \\ &= Var\{r^N(m)\} + \frac{\sigma^2(\sigma^2+2P)}{N} \end{aligned} \qquad [23]$$

where P is the average signal power. Once again, the total noise power consists of a systematic noise term and a measurement noise term.

Systematic Noise in $k_1^N(m)$

The variance of $k_1^N(m)$, $Var\{k_1^N(m)\}$, can be obtained theoretically using Eqs. [14] and [16] by solving the stochastic difference equation (Eq. [I-5]) for a specific excitation sequence. The results cannot be expressed in simple closed forms, but can be calculated numerically (*19*). The numerical calculation has been done for random flip angle excitation using Gaussian white noise and random quadrature excitation using random binary sequences. Random flip angle excitation utilizes RF pulses that have random flip angle, but fixed RF phase (see Part I). The variance has also been estimated by Monte Carlo simulations for all three excitation schemes: random flip angle, random quadrature and random phase excitation.

Figure 2a shows the calculated variance of $k_1^N(m)$ with random flip angle excitation using Gaussian white noise and random quadrature excitation using a zero mean random binary sequence for different values of N. The variance is inversely proportional to N and for any given N the variance approaches a constant value as m is increased. The oscillation at small m for the random flip angle excitation has the same frequency as the resonance offset. It does not occur for random

quadrature excitation since the variance of $k_1^N(m)$ with random quadrature excitation is independent of the resonance offset. Figure 2b shows the agreement between the analytical results and Monte Carlo simulations for random flip angle excitation.

As shown in Fig. 2 the variance of $k_1^N(m)$ is a function of m, but it is reasonably flat for a large range of m. Define the systematic noise power as the average variance:

$$\begin{aligned} P_{sn} &= \lim_{M\to\infty} \frac{1}{M} \sum_{m=0}^{M-1} Var\{k_1^N(m)\} \\ &= Var\{k_1^N(\infty)\}, \end{aligned} \qquad [24]$$

where $Var\{k_1^N(\infty)\}$ is well defined and is inversely proportional to N as shown in Fig. 2. It was shown in Part I that $K_1(\omega)$ is Lorentzian when the excitation power is low. This implies that $k_1(m)$ is an exponentially decaying sinusoid with an amplitude $|k_1(0)|$. Define the signal-to-systematic-noise ratio as

$$(S/N)_{sn} = \frac{|k_1(0)|^2}{Var\{k_1^N(\infty)\}}. \qquad [25]$$

Figure 3 contains log-log plot of a Monte Carlo simulation of the signal-to-systematic-noise ratio versus N for random flip angle excitation with three different random sequences. Figure 3a, obtained with Gaussian white noise, shows that the systematic noise power is inversely proportional to N. Figure 3b was obtained with sub-sequences generated by a 31-bit MLS generator. The length of the sub-sequences was much smaller than $2^{31} - 1$, the period of the generator. Such sub-sequences behave just like random binary sequences, resulting in a plot very similar to that for the Gaussian white noise. Figure 3c was obtained with sub-sequences generated by a 15-bit MLS generator. There is a gain of almost 20dB in signal-to-systematic-noise ratio when N is a multiple of $2^{15} - 1$, the period of the 15-bit MLS generator. This behavior is a consequence of the auto-correlation of the complete MLS being a delta function with a small negative offset. The log-log plot of the Monte Carlo simulations of the signal-to-systematic-noise ratio versus N for random quadrature excitation are almost identical to those in Fig. 3. The corresponding plot for random phase excitation with a uniformly distributed sequence closely resembles that in Fig. 3a.

Systematic Noise in $r^N(m)$

Monte Carlo simulations show that $Var\{r^N(m)\}$ is very similar to $Var\{k_1^N(m)\}$. For $r^N(m)$, define the systematic noise power as the average variance:

$$\begin{aligned} P_{sn} &= \lim_{M\to\infty} \frac{1}{M} \sum_{m=0}^{M-1} Var\{r^N(m)\} \\ &= Var\{r^N(\infty)\}, \end{aligned} \qquad [26]$$

where $Var\{r^N(\infty)\}$ is well defined. The signal-to-systematic-noise ratio is defined as

$$(S/N)_{sn} = \frac{P^2}{Var\{r_1^N(\infty)\}}. \qquad [27]$$

The log-log plots of the signal-to-systematic-noise ratio versus N for the three different random sequences obtained by Monte Carlo simulations are also shown in Fig. 3. The plots show that the systematic noise power is again inversely proportional to N when the excitation sequence is a Gaussian white noise or a sub-sequence generated by a 31-bit MLS generator. The systematic noise power drops substantially when N is a multiple of the period of the 15-bit MLS generator. For arbitrary N and a given type of excitation the signal-to-systematic-noise ratio for $r^N(m)$ is approximately 3dB lower than for $k_1^N(m)$. When a 15-bit MLS generator is used and N is a multiple of the period, the difference is approximately 6dB lower. This is a disadvantage of using the signal power spectrum to approximate the true spectrum. The signal-to-systematic-noise ratio of the signal power spectrum for random quadrature excitation and random phase excitation are once again almost identical to those in Fig .3.

Nonlinear Systematic Noise With MLS Excitations

The expressions for $K_1(\omega)$ for the three different excitation schemes predict three possible types of spectral distortion: a line broadening, a shift in resonance offset and a non-uniform response across the spectrum. However, in 1982 Blümich and Ziessow (*8*) showed that noise-like distortion might result from excitations with MLS at high power. They attributed the distortion to linear processing

of a nonlinear spin response and used a heuristic ansatz for the Volterra kernels to describe the distortion. The following analysis will show that the distortion is actually due to characteristics of the MLS which are manifest in $k_1(m)$ and $K_1(\omega)$ when the spin system is driven into a nonlinear regime with high excitation power.

The Monte Carlo simulated line shapes of $K_1(\omega)$ for random flip angle excitation using zero mean binary MLS are shown in Fig. 4a. As the RMS flip angle is increased, there is an increase in the relative amount of noise-like distortion in addition to line broadening and a notch artifact. This agrees with Blümich and Ziessow's experimental observations. The systematic noise due to the variance of $k_1(m)$ in these plots should be negligible since N(=512000) is very large. There is less noise-like distortion when a Gaussian white noise generator is used, as shown in Fig. 4b. A comparison of $k_1(m)$ generated with MLS and Gaussian white noise, in Fig. 5, shows that the noise-like distortion with MLS excitation is due to spurious components at $m = 62, 143$ and 255. The theory discussed in previous sections for random binary sequences does not predict these spurious components. They are artifacts resulting from the properties of the MLS.

A random binary sequence $\alpha(n)$ that takes on the values ± 1 equally likely should have a zero third order auto-correlation:

$$\langle \alpha(n)\, \alpha(n-i)\, \alpha(n-j) \rangle \equiv 0. \qquad [28]$$

Figure 6 is a plot of $\langle \alpha(n)\, \alpha(n-i)\, \alpha(n-j) \rangle$ calculated numerically over a range of i and j values for a sub-sequence generated by a 31-bit MLS generator. It shows that the third order auto-correlation is zero almost everywhere except at (i, j) = (3,31), (31,3), (6,62), (62,6), (12,124) and (124,12), where it has a value of 1. The spikes at (6,62) and (62,6) are related to the spurious component of $k_1(m)$ at $m = 62$.

The fact that a spike occurs at $(31, 3)$ is a direct consequence of the algorithm used by the 31-bit

MLS generator. Figure 7 is a block diagram of the 31-bit MLS generator. The generator consists of a 31-bit shift register with the exclusive-OR of the 31st bit and the 3rd bit fed back to form the 0th bit, the bit at the input of the register SR1. Therefore the 0th, 3rd and 31st bits of the MLS are highly correlated, giving rise to the spikes at (31,3) and (3,31). Similarly, the 1st, 4th and 32nd bits are also highly correlated. By propagating this triplet along the sequence, it can be shown that the 0th, 6th and 62nd bits are also highly correlated, giving rise to the spikes at (62,6) and (6,62). This indicates that the spikes are MLS generator dependent and are not due to the use of sub-sequences. No spikes appear in the third order auto-correlation of a sequence generated by the Gaussian white noise generator used to obtained Fig. 4b.

The fourth order auto-correlation is

$$\langle \alpha(n)\,\alpha(n-i)\,\alpha(n-j)\,\alpha(n-l)\rangle = 0 \qquad [29]$$

when l is strictly bigger than i and j. Calculations of the fourth order auto-correlation of a sub-sequence generated by a 31-bit MLS generator show spikes at (i,j,l) = (3,19,143), (19,3,143), (3,7,255) and (7,3,255). These spikes are related to the spurious components of $k_1(m)$ at $m = 143$ and 255. The reason a spike occurs at (3,19,143) is similar to that for the spike at (62,6) of the third order auto-correlation. The 0th, 3rd, 19th and 143rd bits are highly correlated due to the propagation of the highly correlated triplet, the 0th, 3rd and 31st bits.

The auto-correlations of orders higher than two are related to the nonlinear components of the magnetization response. Consider the random flip angle excitation experiment, wherein the magnetization response can be written as a Volterra series (*20*):

$$\begin{aligned} M_{xy}(n) &= \sum_{j=0}^{\infty} H_j[\alpha(n)] \\ &= h_0 + \sum_{i=0}^{n} h_1(i)\,\alpha(n-i) + \sum_{i=0}^{n}\sum_{j=0}^{n} h_2(i,j)\,\alpha(n-i)\,\alpha(n-j) \\ &\quad + \sum_{i=0}^{n}\sum_{j=0}^{n}\sum_{l=0}^{n} h_3(i,j,l)\,\alpha(n-i)\,\alpha(n-j)\,\alpha(n-l) + \cdots . \end{aligned} \qquad [30]$$

A Volterra series is a generalization of the Taylor series of a function of multiple arguments. The jth order Volterra functional, $H_j[\alpha(n)]$, summarizes the jth order nonlinearity of the magnetization response and is given by a jth order convolution of the input with the jth order Volterra kernel, h_j. For a zero mean excitation sequence $\alpha(n)$, the input-output cross-correlation is given by Eq. [I-8]:

$$\begin{aligned} k_1(m) &= \frac{1}{\alpha^2}\langle M_{xy}(n)\,\alpha(n-m)\rangle \\ &= h_1(m) + \frac{1}{\alpha^2}\sum_{i=0}^{n}\sum_{j=0}^{n} h_2(i,j)\langle\alpha(n-i)\,\alpha(n-j)\,\alpha(n-m)\rangle \\ &\quad + \frac{1}{\alpha^2}\sum_{i=0}^{n}\sum_{j=0}^{n}\sum_{l=0}^{n} h_3(i,j,l)\langle\alpha(n-i)\,\alpha(n-j)\,\alpha(n-l)\,\alpha(n-m)\rangle + \cdots . \end{aligned} \qquad [31]$$

All the even order Volterra kernels are zero for an NMR spin system and do not contribute to $k_1(m)$. When $\alpha(n)$ is a sub-sequence generated by the 31-bit MLS generator in Fig. 7, the unexpected spikes in the fourth order auto-correlation will give rise to terms that depend on the third order Volterra kernel in Eq. [31]. For example, consider the spike at (i,j,l) = (3,19,143), which contributes the following terms to $k_1(m)$:

$$\begin{aligned} &\alpha^2\,[h_3(m+3,m+19,m+143) + h_3(m-3,m+16,m+140) \\ &+h_3(m-16,m-19,m+124) + h_3(m-124,m-140,m-143)]\,. \end{aligned} \qquad [32]$$

The spin system is a causal system so $h_3(i,j,l)$ is zero whenever i,j or l is negative. This implies that the term $h_3(m-124,m-140,m-143)$ does not contribute to $k_1(m)$ until m is bigger than or equal to 143. This explains the spurious component of $k_1(m)$ at $m = 143$. Similarly, the other unexpected spikes in the fourth order auto-correlation will generate terms of the form $h_3(m-137,m-140,m-255)$ and $h_3(m-140,m-137,m-255)$ that give rise to the spurious component of $k_1(m)$ at $m = 255$. When the excitation power is low, the magnetization response is linear with respect to the excitation and the higher order Volterra kernels are insignificant compared to the linear kernel h_1. Therefore, the unexpected spikes in the higher order auto-correlations of the MLS do not cause significant spurious components in $k_1(m)$. However, when the excitation power is increased, the higher order nonlinear components in the magnetization response become

larger than the linear component and the spurious components in $k_1(m)$ are observed.

For one dimensional NMR spectroscopy, the excitation power level that gives the maximum signal-to-noise ratio is usually sufficiently small that the magnetization response is roughly linear, therefore, the spikes in the higher order auto-correlations of the MLS do not cause significant noise-like distortion in the reconstructed spectrum. However, these features will make the interpretation of multi-dimensional stochastic NMR spectroscopic data very difficult since the multi-dimensional NMR information is related to higher order Volterra kernels. One way to reduce the amount of noise-like distortion for a given excitation power is to use a different MLS generator. For example, a 19-bit MLS generator consists of a 19-bit shift register with the exclusive-OR of the 1st, 2nd, 5th and 19th bits fed back to form the 0th bit. Erroneous spikes will only occur in auto-correlations of order 5 or higher, therefore, only Volterra kernels of order 5 or higher will contribute spurious components to $k_1(m)$. As shown in Part I the integrated line intensity decreases rapidly as the excitation power is increased, i.e. as the system becomes more nonlinear; this means that the nonlinear components of the magnetization response decrease rapidly with the order of the nonlinearity. Hence, the spurious components generated by the 5th order Volterra kernel are usually much smaller than those generated by the 3rd and the 4th order kernels. Consequently there will be less noise-like distortion when the 19-bit MLS is used. This is demonstrated by the results of a Monte Carlo simulation of $K_1(\omega)$ shown in Fig. 8, where the lines have much less noise-like distortion than those in Fig. 4a. A 30-bit MLS generator also has this desirable property. One additional advantage of using the 19-bit MLS is that the period (=524287) is not prohibitively long and so the entire MLS can be used to achieve the 20dB gain in signal-to-systematic-noise ratio over excitations with Gaussian white noise or random binary sequences.

Experimental Verification

The experiments were performed on a 0.5T, 1 meter bore, home built imaging system (developed by IBM Corporation, Massachusetts Institute of Technology, and Lawrence Berkeley Laboratory). A circuit was built to interpose two 31-bit MLS generators between the pulse programmer and transmitter to implement binary MLS excitation (*19*). The sample was a 10cm sphere filled with an aqueous copper sulphate solution. The T_1 and T_2 of the sample were measured to be 160ms and 140ms, respectively. However, due to static field inhomogeneity (1ppm), the effective T_2, T_2^*, was only 45ms. All the experiments used a T_R of 200μs, which corresponds to an optimal RMS flip angle of 2.8°. The RF pulsewidth was 25μs, which gives an excitation bandwidth of about 40kHz. The width of the reconstructed spectrum is $1/T_R$ = 5kHz. The flip angles of the RF pulses were calibrated with a conventional one pulse NMR experiment. The number of data points sampled for each experiment N(=65536) was a very small fraction of the period of the MLS ($2^{31} - 1$), hence the excitation sequence behaves like a random binary sequence. Initial results showed a broad line resulting from the plastic material in the RF probe (*17*). In order to avoid confusion in the interpretation of the spectral line of the copper sulphate solution, the plastic line was obtained for each study and subtracted to correct the baseline.

Figure 9 shows the experimental line shapes of $K_1(\omega)$ and $S(\omega)$, and a plot of the average signal power as a function of the RMS flip angle for the random phase (random quadrature) excitation. The plots are very similar to those in Fig. 1 with three exceptions: (1) There is noise-like distortion in the experimental $K_1(\omega)$, (2) as discussed in the previous sections $S(\omega)$ has a DC offset resulting from the measurement noise and (3) $S(\omega)$ shows insignificant noise-like distortion even when the excitation power is high. Finding noise-like distortion in the experimental $K_1(\omega)$ is not surprising since the experimental excitation sequence is a sub-sequence of a 31-bit MLS, while the theoretical results are obtained for a random binary sequence. The noise-like distortion increases as the RMS flip angle increases, in agreement with Blümich and Ziessow's observations (*8*) and

the Monte Carlo simulated results shown in the previous section (Fig. 4a). The fact that $S(\omega)$ shows insignificant noise-like distortion is an advantage of $S(\omega)$ over $K_1(\omega)$ as an estimate of the spectrum. Also notice that neither $K_1(\omega)$ nor $S(\omega)$ has a notch artifact.

Monte Carlo simulations of $k_1(m)$ in the previous section show spurious components at $m = 62$, 143 and 255 when a 31-bit MLS generator is used. Figure 10 shows the real part of $k_1(m)$ obtained experimentally for random flip angle excitation with a 31-bit MLS generator. It is very similar to the Monte Carlo simulated results in Fig. 5 even though T_1, T_2 and the acquisition parameters are different. The spurious components are indeed at $m = 62$, 143 and 255.

Conclusion

Analysis in Part I (*17*) showed that the spectrum obtained with random flip angle excitation has several different saturation artifacts: a line broadening that varies with the resonance offset, a slight shift in resonance offset and a notch at the negative of the resonance offset. To minimize the non-uniformity in line broadening, a sub-optimal RMS flip angle must be used. In order to improve on these results, two new excitation schemes have been introduced, the random phase excitation and the random quadrature excitation. The random RF phase of both excitations removes the shift in resonance offset and the notch artifact, and gives a uniform line broadening across the spectrum. The line broadening results in a loss of resolution, but it is predictable and does not affect the integrated line intensity.

The random phase excitation and the random quadrature excitation give an average signal power that is independent of the resonance offset. The signal-to-noise ratio is maximized when α_{max} is approximately the Ernst angle, $\cos^{-1}(e^{-T_R/T_1})$. For RMS flip angles up to α_{max}, the performance of the two excitations are identical and both the Fourier transform of the input-output cross-correlation and the signal power spectrum are good estimates of the true spectrum. In addi-

tion, α_{max} is usually one to two orders of magnitude smaller than the Ernst angle for a conventional pulsed FT-NMR experiment with $T_R \approx T_1$. This corresponds to a reduction of the peak RF power requirement by a factor of 10^2 to 10^4 when compared to the conventional pulsed FT-NMR experiments.

The stochastic experiment provides two estimators of the spectrum, the Fourier transform of the input-output cross-correlation, $K_1(\omega)$, and the signal power spectrum $S(\omega)$. At low excitation power, such that the magnetization response is linear, both $K_1(\omega)$ and $S(\omega)$ are good estimates of the real spectrum. At higher excitation power, they show slightly different saturation characteristics. The advantages of $S(\omega)$ over $K_1(\omega)$ are: (1) $S(\omega)$ is obtained directly from the signal, and so the excitation sequence need not be stored or regenerated for the reconstruction, simplifing hardware and software design, (2) in the case of random flip angle excitation, the notch artifact is less pronounced in $S(\omega)$ (see Part I), (3) $S(\omega)$ shows much less noise-like distortion and (4) $S(\omega)$ will appear smoother and less noisy than $K_1(\omega)$ when the measurement noise is the dominating noise source because white measurement noise will behave as white noise in $K_1(\omega)$, whereas this noise appears as a DC offset in $S(\omega)$. The disadvantages are: (1) The signal-to-systematic-noise ratio is approximately 3dB lower for $S(\omega)$ than for $K_1(\omega)$, (2) The $S(\omega)$ of two nearby spectral lines interact nonlinearly in the overlapping region (see Part I) and (3) the measurement noise is transformed to a process consisting mainly of a DC offset. The non-white systematic noise may result in observable structural artifacts when the signal-to-measurement-noise ratio is low. A longer signal sequence, i.e. a large N, must be used to guarantee a higher signal-to-measurement-noise ratio.

Theoretical analysis shows that at the optimal excitation power that maximizes the average signal power, random binary sequences and Gaussian white noise sequences give almost identical spectral response (see Part I). The major advantage of random binary sequences over Gaussian

white noise sequences is that random binary sequences can be approximated by maximum length sequences (MLS) with the following advantages. (1) MLS is inexpensive to generate with hardware and software. The sequence can be regenerated any time it is needed. (2) The binary nature simplifies the computations of cross-correlations and auto-correlations. Time consuming multiplication operations can be replaced by simple additions and subtractions in the Fast Hadamard Transform algorithms. The computation time is shorter than that required for Fast Fourier Transform algorithms. (3) The periodic nature of MLS allows coherent signal averaging to improve the S/N ratio. (4) When Gaussian white noise sequences or truly random binary sequences are used, the systematic noise power is inversely proportional to N, the total number of signal points used to calculate the cross-correlation and auto-correlation by time averaging. However, when a MLS is used and N is equal to an integral multiple of the period of the MLS there is a gain of approximately 20dB in the signal-to-systematic-noise ratio over Gaussian white noise sequences and truly random binary sequences of similar length.

However, one must observe some precautions when using MLS. The sum of a full MLS that takes on the values $\pm\alpha$ is non-zero. Therefore, if the product of the period of the MLS and T_R is comparable or shorter than T_1 and T_2, the magnetization response may acquire a non-zero steady state component that results in an artifact at the negative of the resonance offset and a non-uniform response across the spectrum (*19*). If this is the case, a MLS with a longer period must be used. This may result in a large N. The auto-correlations of high orders may have unexpected generator-dependent spikes. These spikes excite high order nonlinear components of the spin system and cause noise-like distortion to be introduced into the Fourier transform of the input-output cross-correlation when the excitation power is high. The amount of noise-like distortion is usually insignificant at the power level that maximizes the S/N ratio, i.e. when the magnetization response is nearly linear. One way to reduce the noise-like distortion for a given excitation power is to use a MLS generator that has more bits being fed back to form the 0th bit (Fig 7). The noise-like distor-

tion can also be reduced significantly by using the signal power spectrum to approximate the real spectrum.

Finally it has been shown that stochastic NMR with random phase excitation or random quadrature excitation using MLS is simple to implement and is an effective technique for high field NMR studies. This is particularly relevant for *in vivo* studies.

Acknowledgements

This work was supported in part by the Whittaker Foundation (Mark S. Roos) and the U.S. Department of Energy under contract No. DE-AC03-76SF00098.

References

1. R. R. Ernst, *J. Magn. Reson.* **3**, 10(1970).

2. R. Kaiser, *J. Magn. Reson.* **3**, 28(1970).

3. R. Kaiser, *J. Magn. Reson.* **15**, 44(1974).

4. E. Bartholdi, A. Wokaun and R. R. Ernst, *Chem. Phys.* **18**, 57(1976).

5. R. Kaiser and W. R. Knight, *J. Magn. Reson.* **50**, 467(1982).

6. W. R. Knight and R. Kaiser, *J. Magn. Reson.* **48**, 293(1982).

7. B. Blümich and D. Ziessow, *Ber. Bunsenges. Phys. Chem.* **84**, 1090(1980).

8. B. Blümich and D. Ziessow, *J. Magn. Reson.* **46**, 385(1982).

9. B. Blümich and D. Ziessow, *J. Magn. Reson.* **52**, 42(1983).

10. B. Blümich and R. Kaiser, *J. Magn. Reson.* **54**, 486(1983).

11. B. Blümich and D. Ziessow, *Molec. Phys.* **48**, 955(1983).

12. B. Blümich and D. Ziessow, *Molec. Phys.* **48**, 969(1983).

13. B. Blümich and D. Ziessow, *J. Chem. Phys.* **78**, 1059(1983).

14. B. Blümich, *Molec. Phys.* **51**, 1283(1984).

15. B. Blümich, *J. Magn. Reson.* **60**, 37(1984).

16. D. Chaudhuri,"Hadamard Zeugmatography Using 3-D Projection Reconstruction", Master's thesis, State University of New York at Stony Brook, August 1986.

17. S. T. S. Wong, M. S. Roos, R. D. Newmark and T. F. Budinger, submitted to *J. Magn. Reson.*.

18. I. S. Gradshteyn, I. M. Ryzhik, "Table of Integrals, Series and Products", Academic Press, 1980.

19. S. T. S. Wong, "Discrete Analysis of Stochastic NMR", Ph.D. thesis, University of California, San Francisco, December 1988.

20. M. Schetzen, "The Volterra and Wiener Theories of Nonlinear System", John Wiley & Sons, 1980.

Figure Captions

Figure 1 (a) Line shape (absorption part) of $K_1(\omega)$, (b) $S(\omega)$ and (c) the average signal power for random quadrature excitation with different RMS flip angle α. $T_1 = 0.5$s, $T_2 = 10$ms, $T_R = 0.1$ms and $\nu = 250$Hz.

Figure 2 (a) Theoretical variance of $k_1^N(m)$ for random flip angle excitation using Gaussian white noise (solid) and random quadrature excitation using a random binary sequence (dotted). (b) Theoretical (dotted) and Monte Carlo simulated (solid) variance of $k_1^N(m)$ for random flip angle excitation using Gaussian white noise with $N = 25600$. $T_1 = 0.5$s, $T_2 = 10$ms, $T_R = 0.1$ms, $\nu = 250$Hz and $\alpha = 1.15°$.

Figure 3 Monte Carlo simulated log-log plot of the signal-to-systematic-noise ratio of $k_1^N(m)$ (*) and $r^N(m)$ (o) versus N for random flip angle excitations. The excitation sequences are (a) Gaussian white noise, (b) 31-bit MLS and (c) 15-bit MLS. $T_1 = 0.5$s, $T_2 = 10$ms, $T_R = 0.1$ms, $\nu = 250$Hz, and a RMS flip angle of $1.15°$.

Figure 4 Monte Carlo simulated line shapes of $K_1(\omega)$ for random flip angle excitation with sub-sequences generated by (a) a 31-bit MLS generator and (b) a Gaussian white noise generator. $T_1 = 0.5$s, $T_2 = 10$ms, $T_R = 0.1$ms, $\nu = 2500$Hz and $N = 512000$.

Figure 5 Monte Carlo simulated real part of $k_1(m)$ for random flip angle excitation with sub-sequences generated by (a) a Gaussian white noise generator and (b) a 31-bit MLS generator. $T_1 = 0.5$s, $T_2 = 10$ms, $T_R = 0.1$ms, $\nu = 2500$Hz, $\alpha = 25°$ and $N = 512000$.

Figure 6 Numerically calculated third order auto-correlation of a sub-sequence generated by a 31-bit MLS generator. The sequence takes on the values ± 1. $N = 20000$.

Figure 7 A 31-bit MLS generator implemented with a 31-bit shift register.

Figure 8 Monte Carlo simulated line shapes of $K_1(\omega)$ for random flip angle excitation with sub-sequences generated by a 19-bit MLS generator. $T_1 = 0.5$s, $T_2 = 10$ms, $T_R = 0.1$ms, $\nu = 2500$Hz and $N = 524287$.

Figure 9 Experimental results. (a) The line shapes of $K_1(\omega)$, (b) $S(\omega)$ and (c) the average signal power for random quadrature/phase excitation obtained with two 31-bit MLS generators. $T_1 = 160$ms, $T_2^* = 45$ms, $T_R = 0.2$ms, $N = 65536$ and $\nu = 60$Hz.

Figure 10 Experimentally obtained real part of $k_1(m)$ for random flip angle excitation with a sub-sequence generated by a 31-bit MLS generator. $T_1 = 160$ms, $T_2^* = 45$ms, $T_R = 0.2$ms, $\nu = 1250$Hz, $N = 65536$ and a RMS flip angle of 24°.

Symbols

o	oh
O	uppercase oh
0	zero
l	ell
1	one
k	lowercase kay
K	uppercase kay
n^{th}	italic n superscript italic th
T_1	italic tee subscript 1
T_2	italic tee subscript 2
θ	theta (Greek)
μ	mu (Greek)
μ_x	mu (Greek) subscript italic x
$\boldsymbol{\mu}_\alpha$	bold mu (Greek) subscript alpha (Greek), a vector
$\boldsymbol{\mu}_M$	bold mu (Greek) subscript italic M
$\boldsymbol{\mu}_R$	bold mu (Greek) subscript italic R
α	alpha (Greek)
α_x	alpha (Greek) subscript italic x
$\boldsymbol{\alpha}$	bold alpha (Greek), a vector
β	beta (Greek)
ω	omega (Greek)
δ_{nm}	delta (Greek) subscript italic nm
Δ	upper case delta (Greek)
ϕ	phi (Greek)

φ_α	variation of phi (Greek) subscript alpha (Greek)
π	pi (Greek)
ν	nu (Greek)
σ	sigma (Greek)
$\boldsymbol{A}$	bold A
$\boldsymbol{B}$	bold B
$\boldsymbol{C}$	bold C
$\boldsymbol{C}_\alpha$	bold C subscript alpha (Greek)
${}_1F_1$	subscript 1 italic F subscript 1
$\mathcal{N}_x$	calligraphic N subscript italic x
$\boldsymbol{\mathcal{N}}$	bold calligraphic N
$\boldsymbol{M}$	bold, italic M, a vector
M_{xy}	italic M subscript italic xy
p_1	p subscript 1
$\boldsymbol{R}_\alpha$	bold R subscript alpha (Greek), a matrix
$\boldsymbol{R}_\theta$	bold R subscript theta (Greek)
$\mathcal{R}e$	calligraphic R and italic e
$\mathcal{Z}$	calligraphic Z

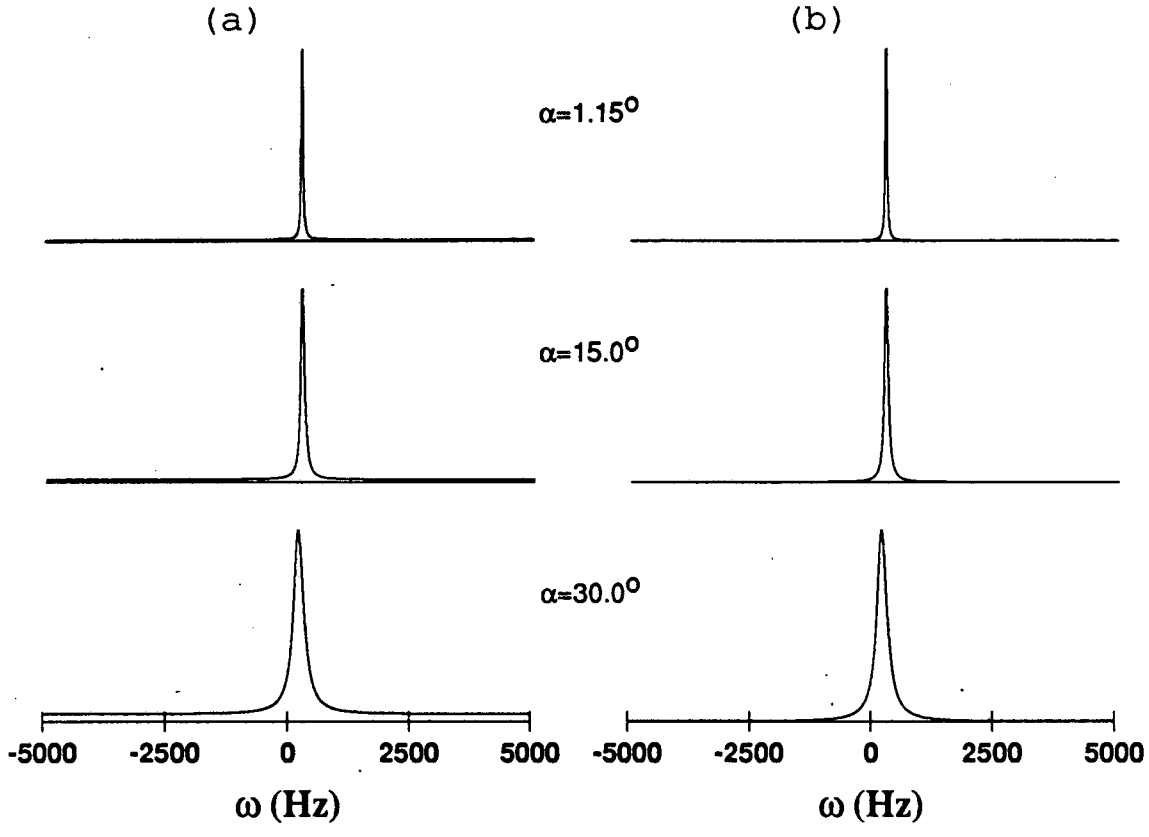
(a)
(b)
α=1.15°
α=15.0°
α=30.0°
-5000
-2500
0
2500
5000
ω (Hz)
-5000
-2500
0
2500
5000
ω (Hz)

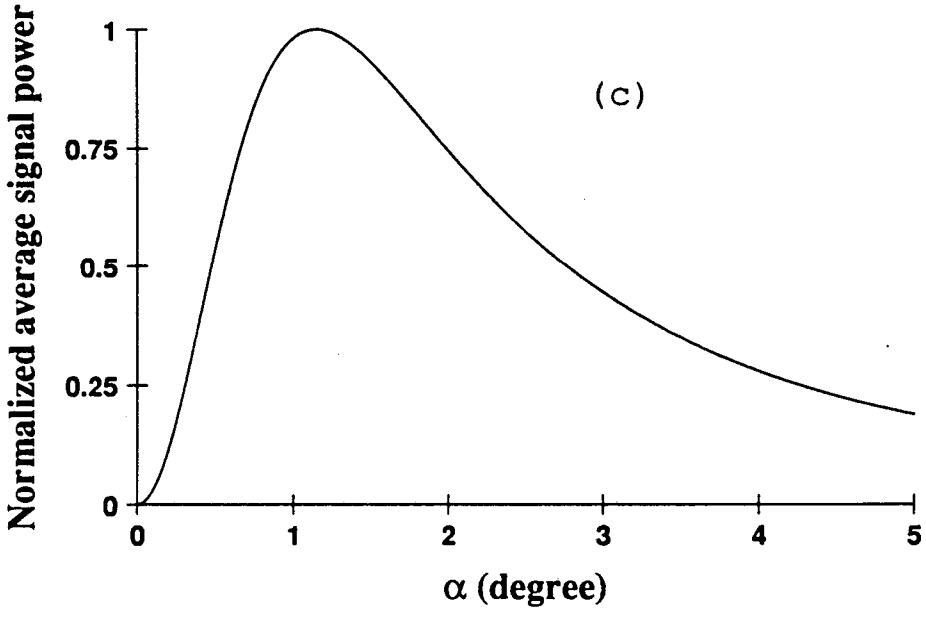
Normalized average signal power
1
0.75
0.5
0.25
0
(c)
0
1
2
3
4
5
α (degree)

(a)

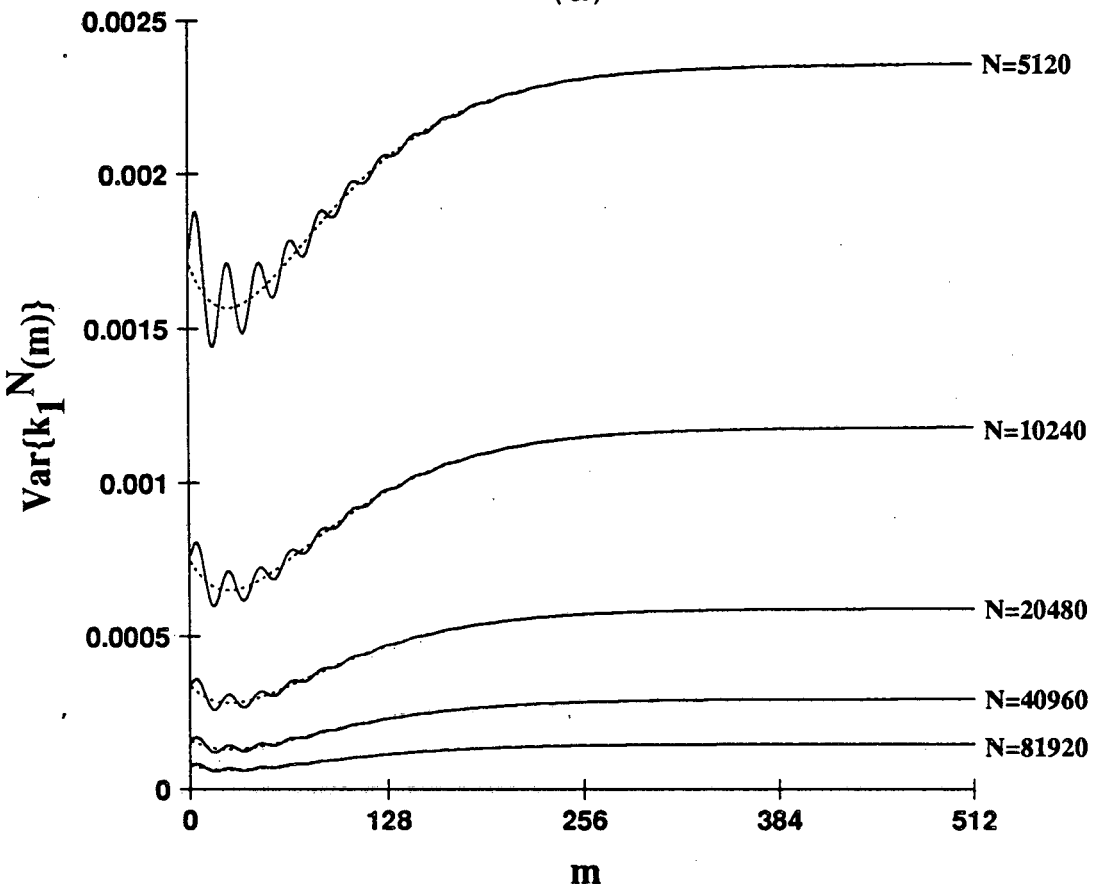
0.0025
0.002
0.0015
0.001
0.0005
0
Var{k1N(m)}
N=5120
N=10240
N=20480
N=40960
N=81920
0
128
256
384
512
m

(b)

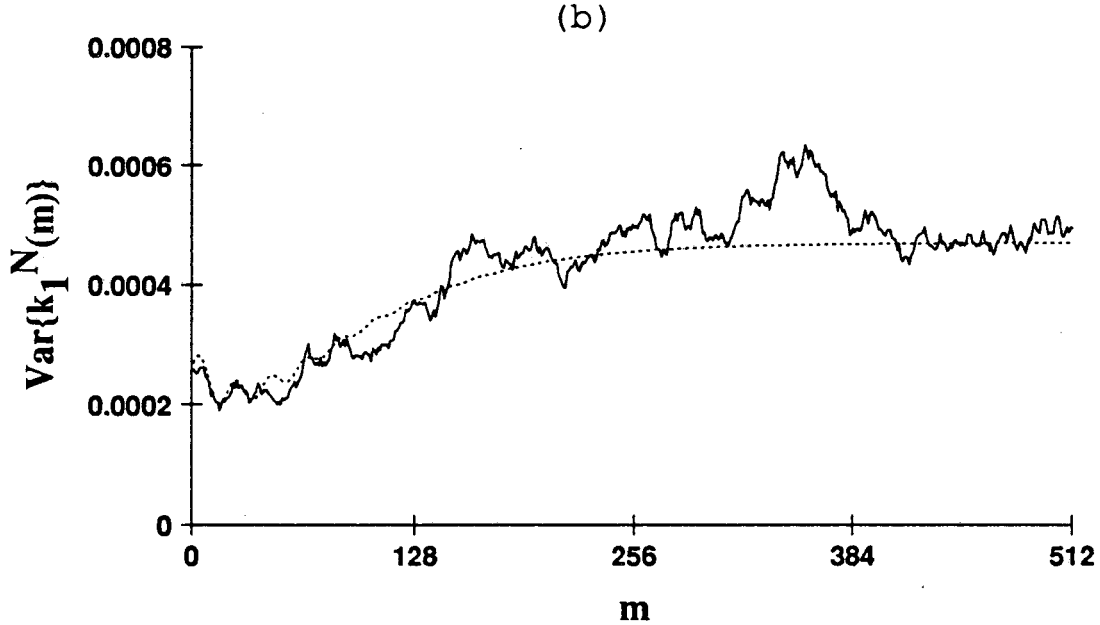
0.0008
0.0006
0.0004
0.0002
0
Var{k1N(m)}
0
128
256
384
512
m

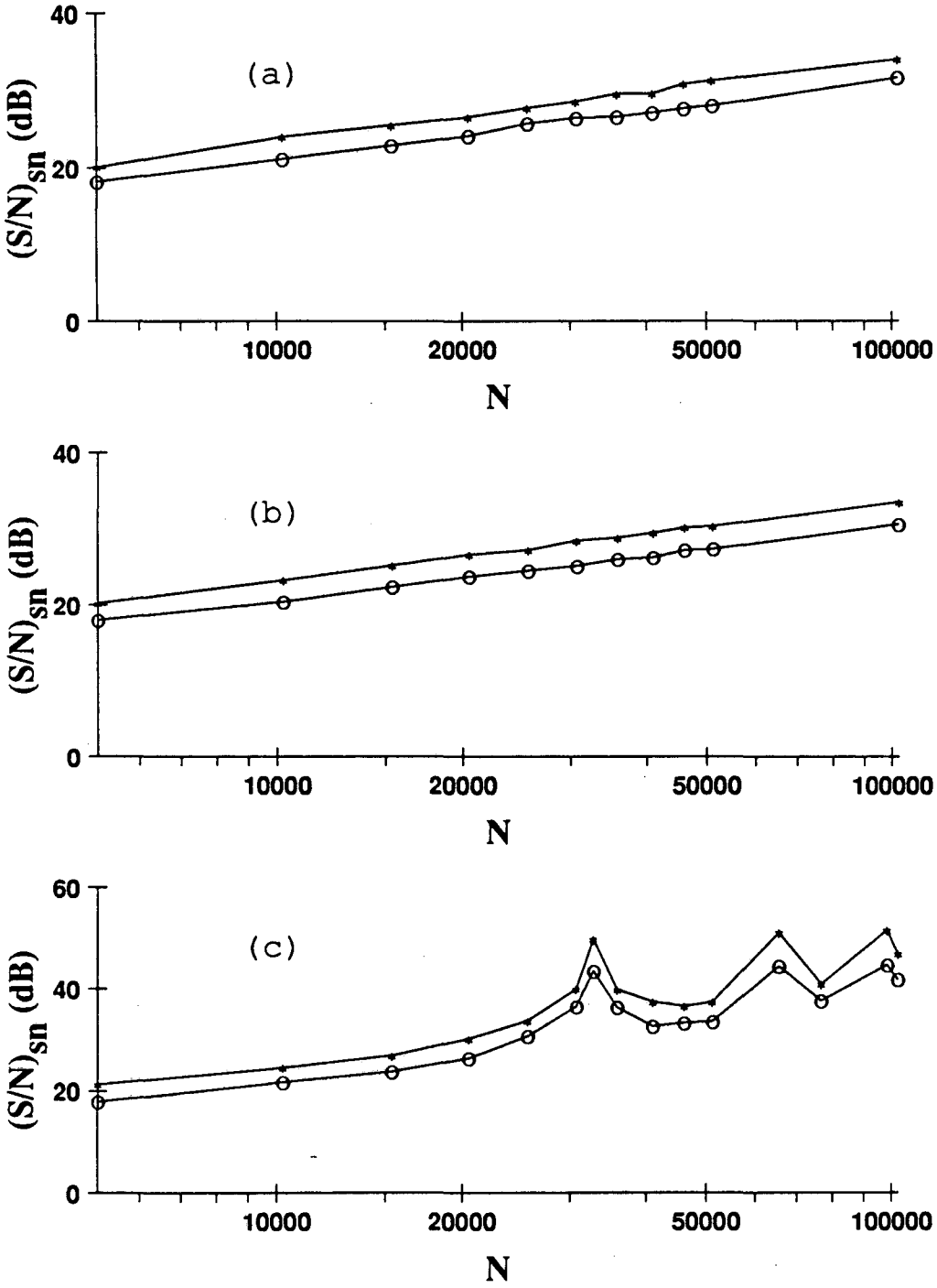
(a)
(b)
(c)
$(S/N)_{sn}$ (dB)
N
0
20
40
60
10000
20000
50000
100000

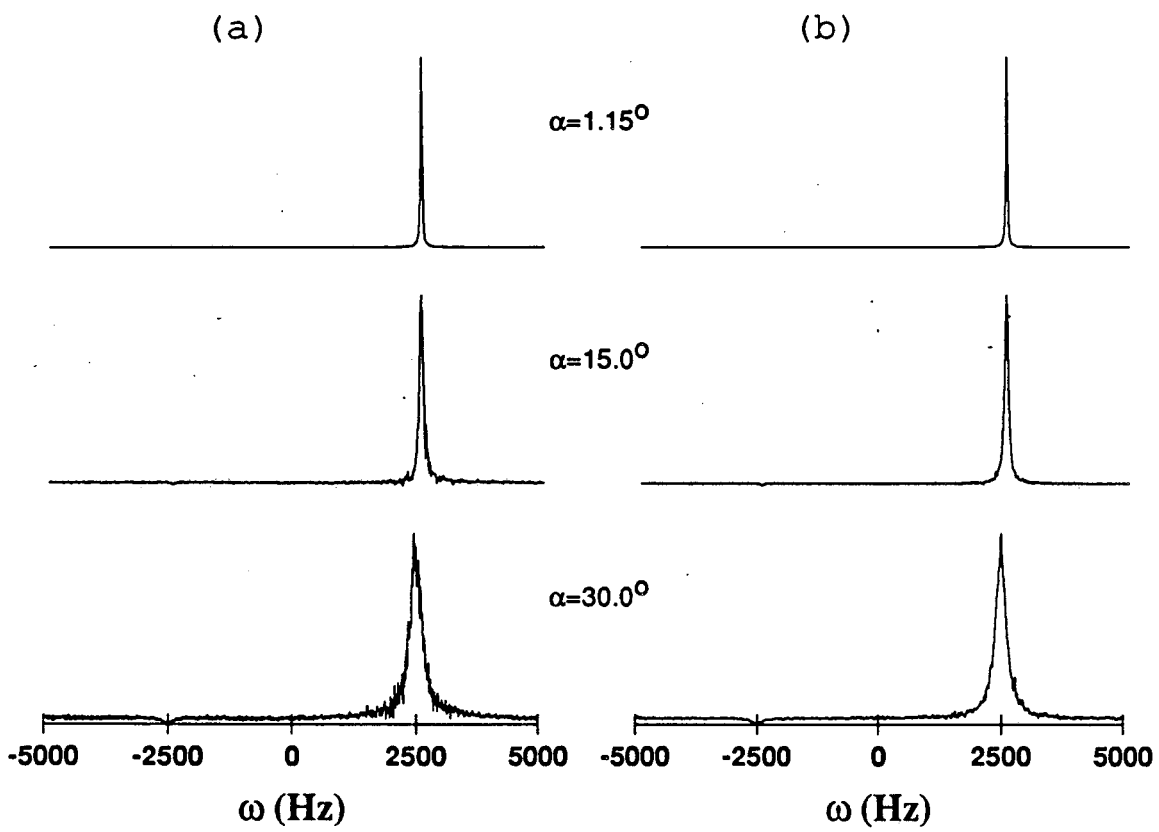
(a)
(b)
α=1.15°
α=15.0°
α=30.0°
-5000
-2500
0
2500
5000
ω (Hz)
-5000
-2500
0
2500
5000
ω (Hz)

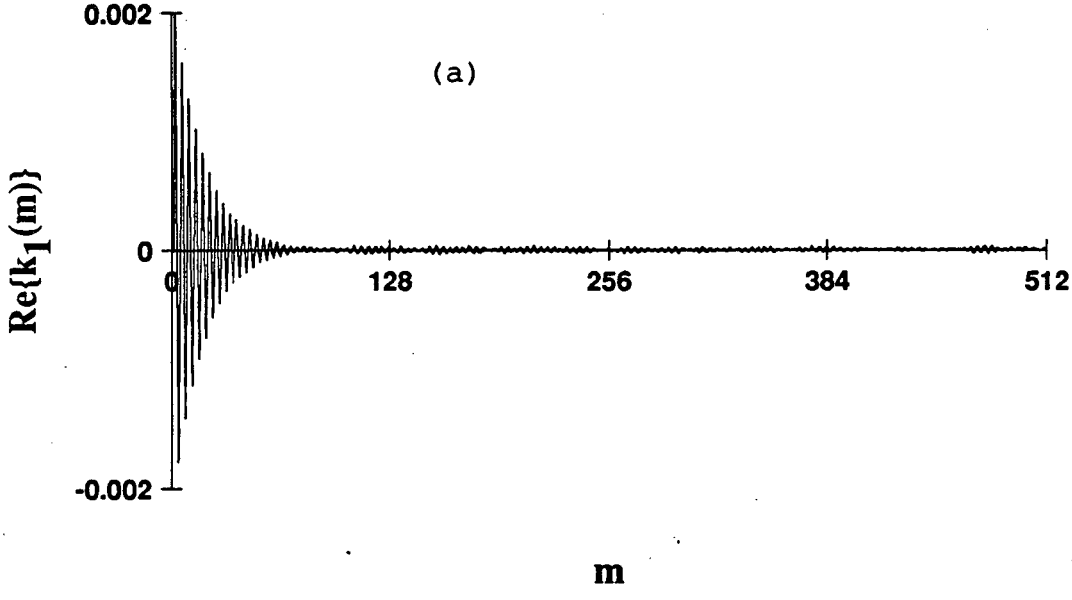
0.002
(a)
Re{k1(m)}
0
0
128
256
384
512
-0.002
m

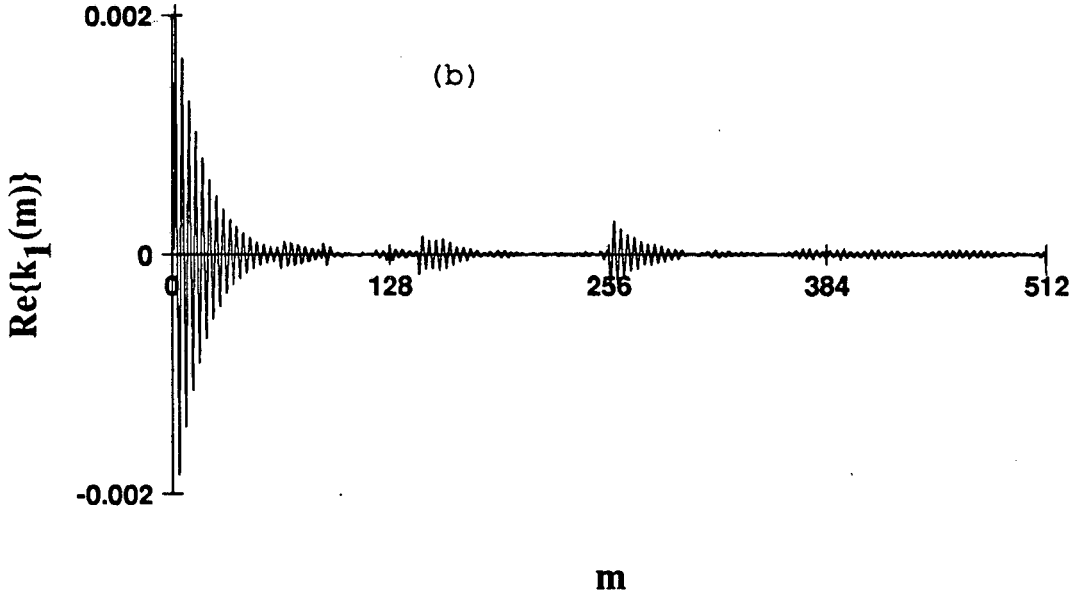
0.002
(b)
Re{k1(m)}
0
0
128
256
384
512
-0.002
m

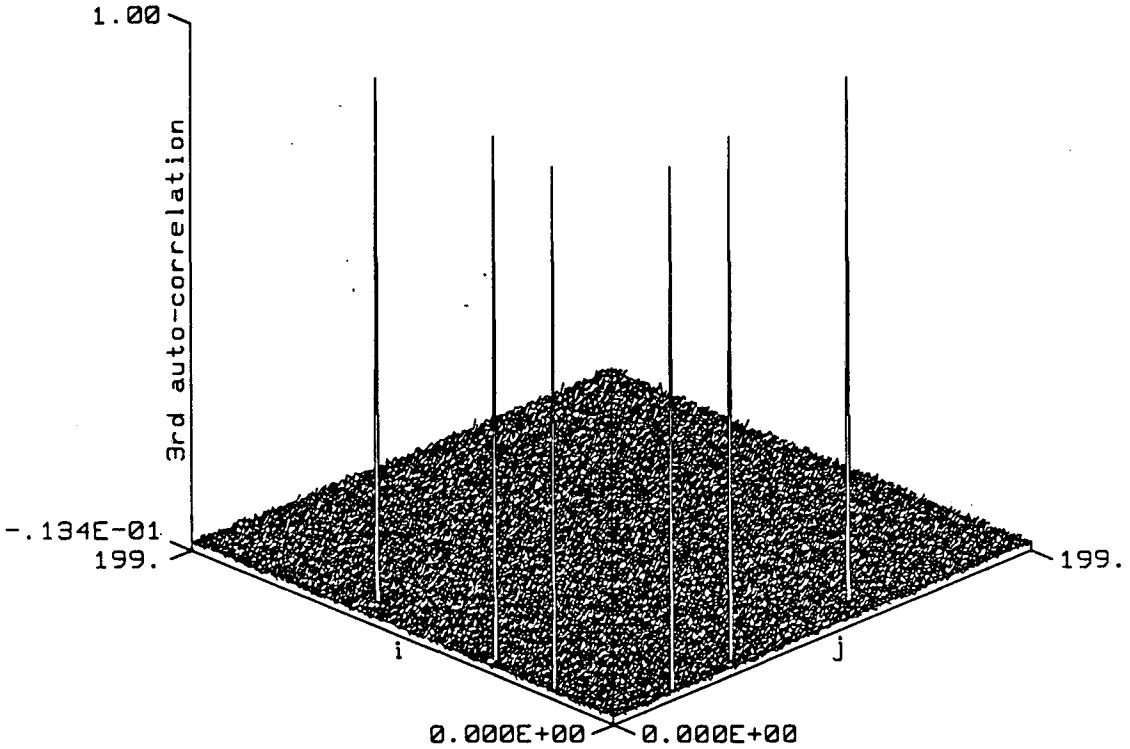
1.00
3rd auto-correlation
-.134E-01
199.
i
0.000E+00
0.000E+00
j
199.

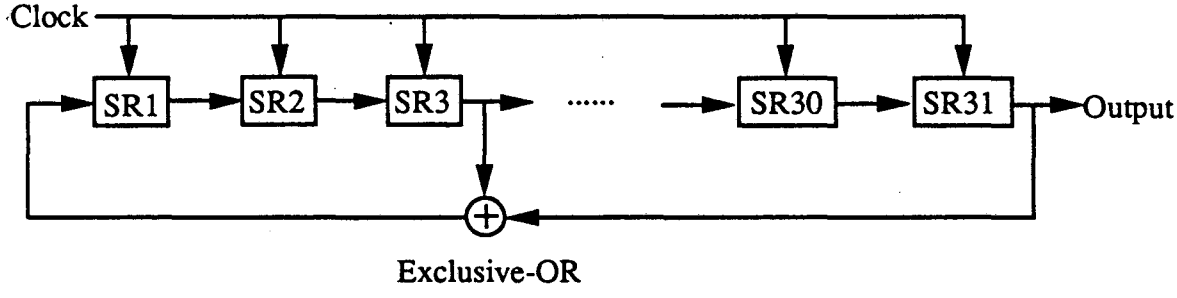
Clock
SR1
SR2
SR3
.....
SR30
SR31
Output
Exclusive-OR

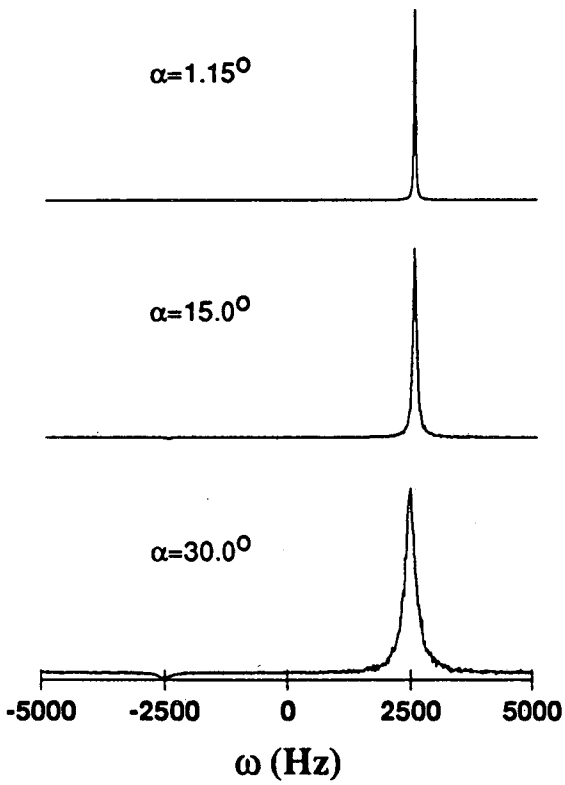
α=1.15°
α=15.0°
α=30.0°
-5000
-2500
0
2500
5000
ω (Hz)

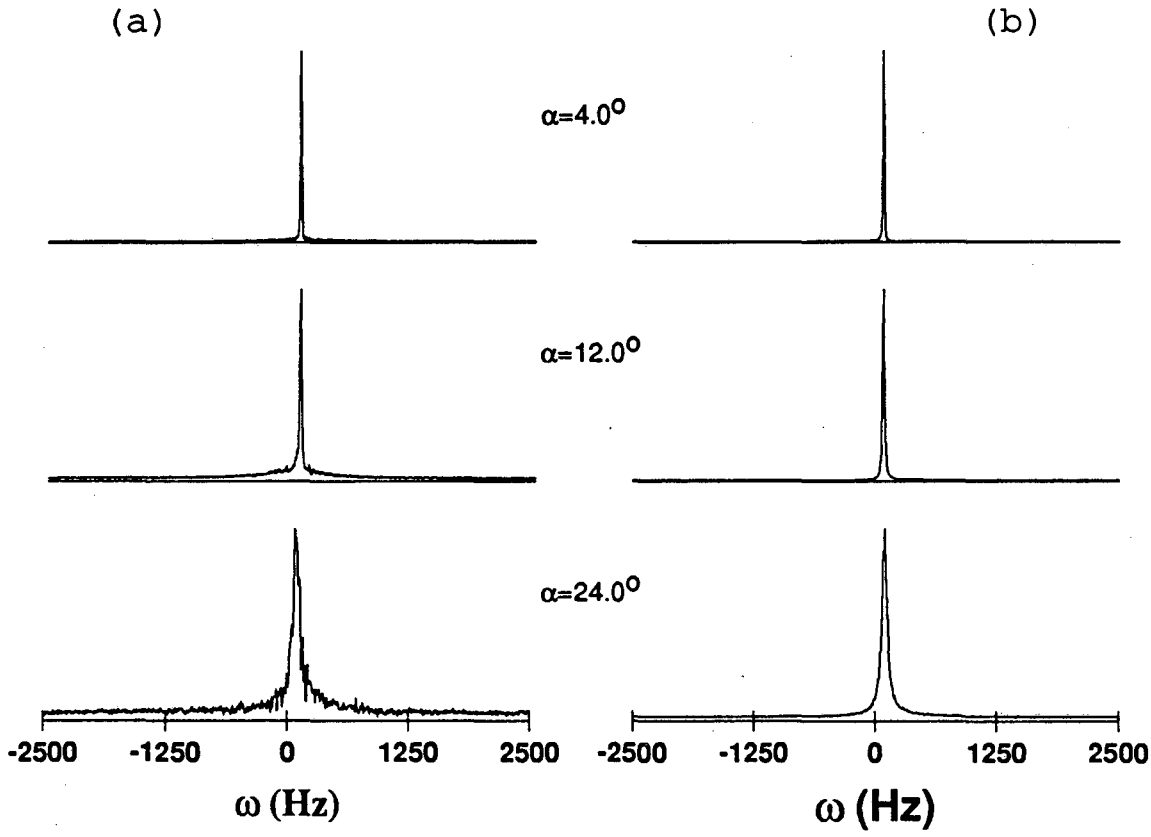
(a)
(b)
α=4.0°
α=12.0°
α=24.0°
-2500
-1250
0
1250
2500
ω (Hz)
ω (Hz)

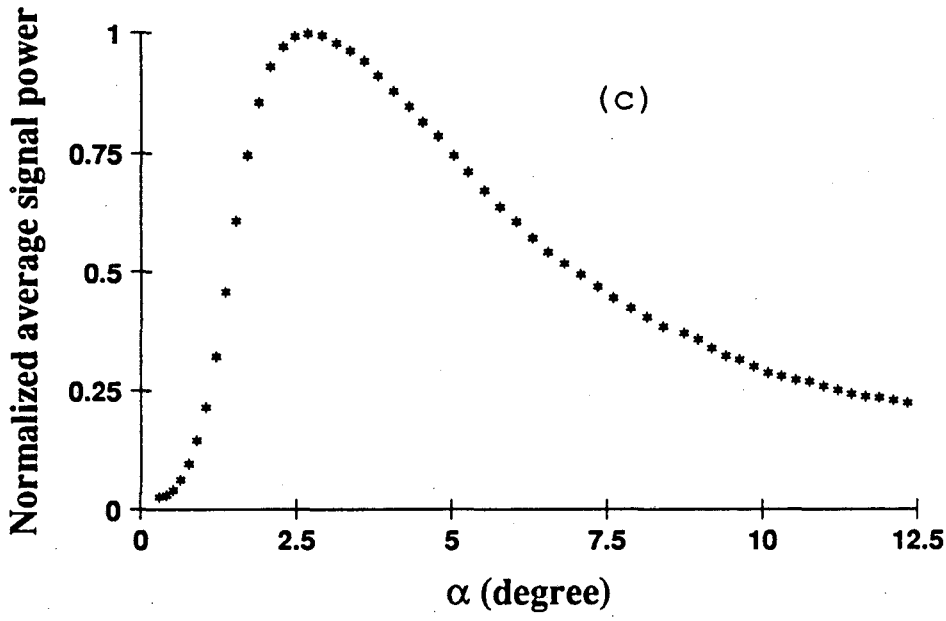
(c)
Normalized average signal power
1
0.75
0.5
0.25
0
0
2.5
5
7.5
10
12.5
α (degree)

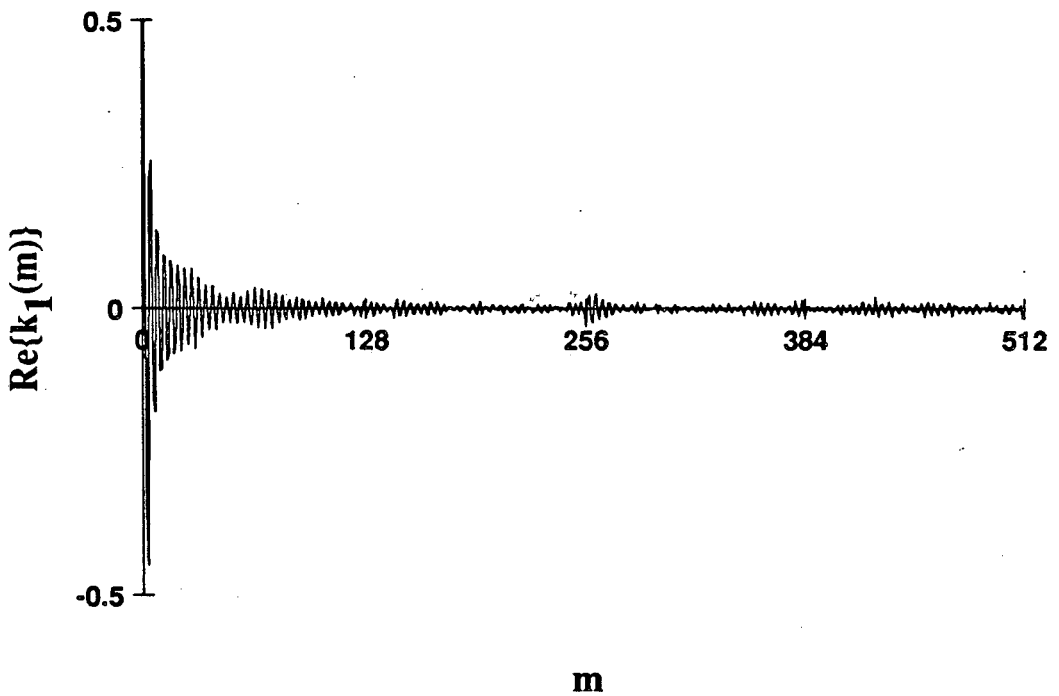
0.5
0
-0.5
0
128
256
384
512
Re{k1(m)}
m

LAWRENCE BERKELEY LABORATORY
TECHNICAL INFORMATION DEPARTMENT
1 CYCLOTRON ROAD
BERKELEY, CALIFORNIA 94720